

Exploiting the causal tensor network structure of quantum processes to efficiently simulate non-Markovian path integrals

Mathias R. Jørgensen*

Department of Physics, Technical University of Denmark, 2800 Kongens Lyngby, Denmark

Felix A. Pollock†

School of Physics and Astronomy, Monash University, Clayton, Victoria 3800, Australia

(Dated: November 15, 2023)

In the path integral formulation of the evolution of an open quantum system coupled to a Gaussian, non-interacting environment, the dynamical contribution of the latter is encoded in an object called the influence functional. Here, we relate the influence functional to the process tensor – a more general representation of a quantum stochastic process – describing the evolution. We then use this connection to motivate an improved tensor network algorithm for the simulation of open systems, building on recent work where the influence functional is represented in terms of time evolving matrix product operators. By exploiting the symmetries of the influence functional, we are able to use our algorithm to achieve orders-of-magnitude improvement in the efficiency of the resulting numerical simulation.

All nanoscale systems are open, and will inevitably interact with their environments. When the system and environment remains largely uncorrelated, a Markovian model of the system dynamics is appropriate [1–3]. In many cases, such as photosynthesis, nanoscale quantum lasers, and quantum thermal machines [4–6], system-environment correlations cannot be ignored. It is then essential to accurately model non-Markovian, or *memory*, effects in the dynamics.

Many techniques have been developed to account for non-Markovian effects, with greater or lesser breadth of applicability. Analytical methods involving time-local equations of motion exist, but are generally highly restricted to specific parameter regimes [7–9]. Often, exact simulation is left to numerical methods, such as those involving discrete path integrals [10–14], time non-local memory kernels [15–18], hierarchical equations of motion [19, 20] and others [21–24]. However, these methods tend to scale unfavourably with both the simulation time and the size of the system in question [25]. Often this makes them inapplicable to important processes involving large complexes or where long time dynamics is important.

Recently, tensor network methods, where underlying structure of linear maps is used to massively reduce the complexity of their description [26], have been applied to the simulation and characterization of open quantum dynamics [27–30]. In particular, Strathearn et al. [31] have shown that discrete path integrals for open systems with Gaussian environments can be recast in terms of matrix product operators; the resulting time-evolving matrix product operator (TEMPO) algorithm is general, numerically exact and has an efficiency comparable to other state of the art methods. By effectively only considering the most important non-Markovian contributions to the dynamics, the algorithm is able to circumvent the exponential memory scaling of the bare path integral representation, in a similar spirit to earlier path-filtering techniques [32–34].

In this paper, we make a formal connection between the path integral structure and the recently developed process tensor framework for characterizing general non-Markovian quantum processes [29]. We then use this to argue for an al-

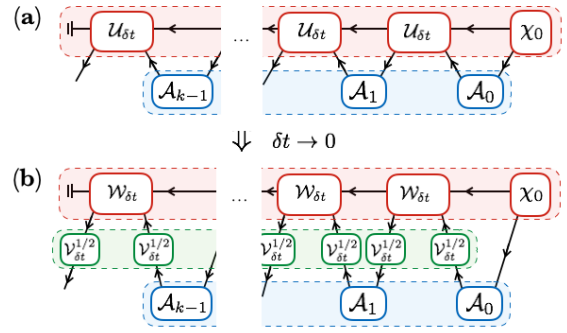


Figure 1. A general quantum process with interventions (top) can be represented as a matrix product form tensor network (red box) that contracts with a filter function consisting of a sequence of superoperators (blue box). This is useful as it makes it possible to separate implemented control operations from the underlying uncontrolled process. In the infinitesimal time step limit (bottom), the uncontrolled process can be further decomposed into free evolution of the system (green box) and a generalized influence functional capturing the influence of the environment.

ternative formulation of the TEMPO algorithm, where we exploit the symmetry of the underlying tensor network to better account for the causality inherent in the dynamics. This alternative formulation is demonstrated to significantly improve the efficiency of the method, which we use to straightforwardly compute non-Markovian emission spectra for the spin-boson model beyond the point where the commonly used quantum regression formula breaks down [35].

Background. – We consider a stationary unitary dynamics on the system we are interested in along with its environment, and suppose the system is transformed by superoperators A_j at the discrete times $\{t_{k-1}, \dots, t_0\}$, which we will take to be at evenly spaced intervals of $\delta t = t_j - t_{j-1}$. In an experiment, these superoperators could correspond to actual interventions on the system as it evolves, i.e. unitary rotations, measurements, etc., in which case they are completely-positive and, if the interventions are not conditional on a particular measure-

ment outcome, trace preserving. Otherwise, as we will see below, the set $\mathbf{A}_{k-1:0} = \{\mathcal{A}_j\}$ could represent more abstract transformations useful in the computation of physical quantities such as operator expectation values or emission spectra. The reduced, potentially unnormalized, state of the system at time t_k is given by

$$\rho_k = \text{tr}_E \{ \mathcal{U}_{\delta t} \mathcal{A}_{k-1} \dots \mathcal{U}_{\delta t} \mathcal{A}_0 [\chi_0] \} , \quad (1)$$

where $\mathcal{U}_{\delta t}$ is a superoperator representation of the unitary evolution of duration δt (for non-stationary dynamics, this would generically depend on the absolute time), and χ_0 is the initial system-environment state. The inclusion of intermediate transformations makes it possible for us to consider a much broader class of physical properties than free evolution of the density operator (corresponding to $\mathcal{A}_j = \mathcal{I}$, the identity superoperator, for all j) would allow, in particular multi-time correlation functions can be studied within this formulation.

From Eq. (1), it is straightforward to see that the state at time t_k is linearly related to each of the set of superoperators $\mathbf{A}_{k-1:0}$ through a mapping, called the process tensor, that depends on the system-environment unitaries and initial state [29]:

$$\rho_k = \mathcal{T}_{k:0} [\mathbf{A}_{k-1:0}] . \quad (2)$$

Unlike in a conventional open quantum systems picture, where density operators are mapped to density operators, this operational formulation stresses that the proper inputs to the description of a quantum process is the set of interventions $\mathbf{A}_{k-1:0}$, and that the intermediate dynamics, and the initial state, are features of the process itself. A representation in terms of process tensors has been shown to consistently generalize the notion of a stochastic process to the quantum case [36], and can be used to define a rigorous Markov condition for quantum processes [37].

In a standard prepare, evolve, measure scenario it is always possible to express the probability of a given outcome as the projection of a state function onto a filter function [38]. A key insight of the process tensor formulation is that this is also possible for more complex across multiple points in time.

Through a generalization of the Choi-Jamiołkowski isomorphism [39], the process tensor can be represented as a many-body state $\Upsilon_{k:0}$. Equation (1) can then be seen as the projection of this onto a filter function $\mathcal{O}_{k-1:0} = A_{k-1}^T \otimes \dots \otimes A_0^T$ comprising the tensor product of Choi states A_j of the superoperators \mathcal{A}_j , such that

$$\rho_k = \text{tr}_A \{ \Upsilon_{k:0} \mathcal{O}_{k-1:0} \} , \quad (3)$$

where the trace is over the $2k$ ancillary spaces corresponding to time steps 0 to $k-1$.

This separation of the process from external interventions is illustrated in Fig. 1, and makes it possible to discuss the simulation of general processes independently of any specific sequence of control operations implemented. It can also be seen in the figure that the process tensor has a natural matrix product form [29] (a fact recently explored in more depth in

Ref. [30] for the case of infinitesimal time steps). This is completely general, and we will now see that it relates to the influence functional of the Feynman-Vernon path integral [40], which can be further decomposed into an efficient tensor network form.

Gaussian influence functional. – Let us now consider the specific structure of the process tensor for Gaussian environments, by which we mean a system-environment Hamiltonian and initial state depending at most quadratically on environment creation and annihilation operators. For concreteness, we focus on spin-boson type models, but our results would extend to fermionic baths as well [41]. Working in natural units ($\hbar = k_B = 1$), we consider a spin system, with Hilbert space dimension d , interacting linearly with a macroscopic bath of harmonic oscillators described by the Hamiltonian

$$\begin{aligned} H &= H_0 + \hat{s} \sum_n (g_n \hat{a}_n + g_n^* \hat{a}_n^\dagger) + \sum_n \omega_n \hat{a}_n^\dagger \hat{a}_n \\ &= H_0 + H_B . \end{aligned} \quad (4)$$

Here, H_0 describes the free spin system and is left arbitrary, and the full bath influence is collected in H_B . A bath mode n has energy ω_n , and is created (annihilated) by the bosonic operator \hat{a}_n^\dagger (\hat{a}_n). The system operator \hat{s} interacts with the bath with coupling constants g_n . Additional linear interaction terms to different system operators could be included, as long as all these system operators commute. But, since such a generalization would not fundamentally alter the structure of the bath influence, we consider only the simplest case. In general, the initial system-environment state could be correlated, but we here take the initial state to be product, such that $\chi_0 = \rho_0 \otimes \tau_\beta$, where the environment is initially described by a thermal state $\tau_\beta = \exp[-\beta \sum \omega_n \hat{a}_n^\dagger \hat{a}_n] / \mathcal{Z}$ at an inverse temperature β , and \mathcal{Z} denotes the partition function. The choice of working with a thermal environment state is not essential, and other Gaussian initial states of the environment could be considered.

In the limit that the time difference δt is small, then the unitary dynamics generated by the Hamiltonian in Eq. (4) can be approximately separated into contributions arising from H_0 and H_B

$$\mathcal{U}_{\delta t} \simeq \mathcal{V}_{\delta t}^{1/2} \mathcal{W}_{\delta t} \mathcal{V}_{\delta t}^{1/2} , \quad (5)$$

where $\mathcal{V}_{\delta t}$ describes the free dynamics and $\mathcal{W}_{\delta t}$ describes the environment influence. The discrepancy between the approximate unitary maps and the actual ones vanishes as $\mathcal{O}(\delta t^3)$ for this symmetric decomposition [42]. Notice that the approximate model does not break unitarity, and so the corresponds to a valid physical process independently of the step size.

Moreover, since there is only a single interaction term in Eq. (4), the interaction unitary preserves the eigenbasis $\{|s\rangle\}$ of the corresponding system operator \hat{s} : $\langle s' | \mathcal{W}_{\delta t} [|s\rangle \langle r |] | r' \rangle = \delta_{ss'} \delta_{rr'} \mathcal{W}_{\delta t}^{(s,r)}$. Together with the decomposition of unitary maps, this allows us to write the approximate process tensor Choi state as

$$\tilde{\Upsilon}_{k:0} = \mathbf{V}_{k:0} [\mathcal{F}_{k:0}] \otimes \rho_0 , \quad (6)$$

where

$$\mathbf{V}_{k:0} = \left(\mathcal{V}_{\delta t}^{1/2} \otimes \mathcal{V}_{\delta t}^{*1/2} \right)^{\otimes k} \quad (7)$$

describes the free unitary dynamics, and

$$\mathcal{F}_{k:0} = \sum_{\vec{s}, \vec{r}} \text{tr}_E \left\{ \mathcal{W}_{\delta t}^{(s_k, r_k)} \dots \mathcal{W}_{\delta t}^{(s_1, r_1)} [\tau\beta] \right\} \times |s_k s_k \dots s_1 s_1 \rangle \langle r_k r_k \dots r_1 r_1| \quad (8)$$

encodes environment induced correlations. $\mathcal{I}_{k:0}$ is an operator representation of the discretized influence functional first introduced by Feynman and Vernon [40] and, for Gaussian environments, the bath degrees of freedom can be traced over analytically using standard path integral techniques [10, 11, 14]. In this case, introducing the d^2 compound indices $\alpha = (s, r)$, an (non-zero) element of the influence functional can be decomposed as

$$\mathcal{F}_{k:0}^{\alpha_k \dots \alpha_1} = \prod_{i=1}^k \prod_{j=1}^i [b_{(i-j)}]^{\alpha_i \alpha_j}, \quad (9)$$

where $b_{(i-j)}$ is called an influence tensor; the exact form, which can often be approximated by an analytic function [43], is given in the Appendix. The influence tensors connect the dynamics around time step i with that around time step j , quantifying the temporal correlations mediated by the environment between those two points, that is they describe memory effects. Since the Hamiltonian is time-independent, the individual tensors $[b_i]$ depend only on the temporal separation $l\delta t$, simplifying the potential complexity considerably. However, since the influence functional is effectively a k index tensor, it is still potentially exponentially complex; we now show how viewing Eq. (9) as a tensor network can make its calculation more tractable.

Tensor network simulation. – The insight of Strathearn et al. in Ref. [31] was that the exponential complexity can often be circumvented because the interaction with the environment will produce approximately finite length correlations in $\mathcal{F}_{k:0}$ in most cases. Such finitely correlated objects have efficient representations as matrix product operators [44]. To introduce this representation we first extend our two-index influence tensors into three-index tensors as $[b_{(i-j)}]^{\gamma\alpha_i}_{\alpha_j} := \delta_{\alpha_j}^{\gamma} [b_{(i-j)}]^{\alpha_i}_{\alpha_j}$, where by convention an upper and a lower repeated index in a product of tensors is summed over (otherwise, tensor elements differing only through raising or lowering are treated as equal). In terms of these, we then define the *non-local* time-evolving matrix product operators

$$\begin{aligned} \mathcal{F}_{k:0}^{\alpha_k \dots \alpha_1} &= \prod_{i=1}^k [b_0]_{\beta_1}^{\alpha_i} \prod_{j=1}^{i-2} [b_j]^{\beta_j}_{\beta_{j+1}} [b_{i-j}]^{\alpha_{i-j}}_{\beta_{j+1}} [b_{i-1}]^{\beta_{i-1}}_{\alpha_1} \\ &= \prod_{i=1}^k \begin{array}{c} \uparrow \alpha_i \\ \bigcirc \\ \downarrow \beta_i \end{array} \leftarrow \begin{array}{c} \uparrow \alpha_{i-1} \\ \bigcirc \\ \downarrow \beta_{i-1} \end{array} \leftarrow \dots \leftarrow \begin{array}{c} \uparrow \alpha_1 \\ \bigcirc \\ \downarrow \beta_1 \end{array}, \end{aligned} \quad (10)$$

where the outgoing (ingoing) arrows in the graphical representation indicate upper (lower) indices, and lines of the same

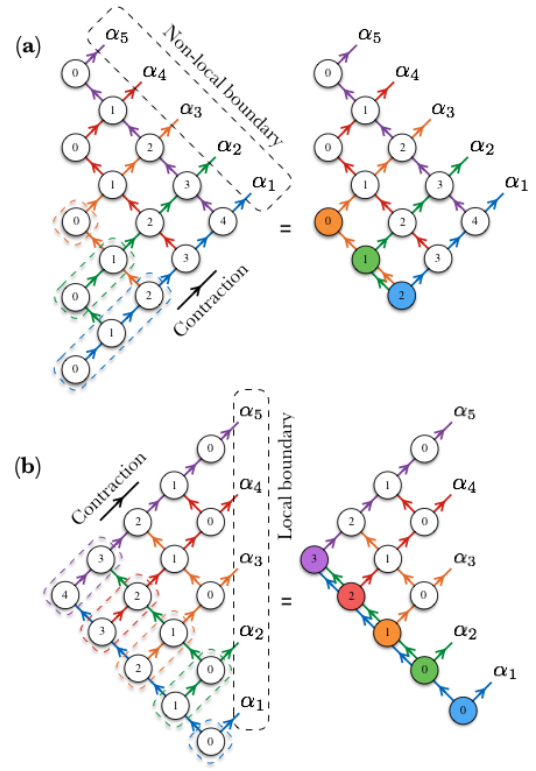


Figure 2. Tensor network representation of the influence functional on five time steps, with nodes representing influence tensors corresponding to the time step separation indicated by their labels. Before contracting the network, indices are constrained to be equal along lines of the same colour; the open boundary can therefore be shifted to any tensor with a similarly coloured leg. (a) With the non-local boundary choice of Ref. [31], the free indices are attached to influence tensors encoding memory effects over all different time-scales. The full network is contracted iteratively down to a boundary matrix product state, layer by layer, with the full influence functional changing at each step. (b) In the local boundary case, considered in detail here, the free indices are always attached to the time-local influence tensors, which typically have the largest singular values. Contraction proceeds as indicated, with the causal influence of each open leg sequentially incorporated into the wider network. The influence functional on an open leg is fixed once the corresponding layer has been contracted over.

colour are fixed to have the same index through Kronecker deltas. At the right boundary of the tensors shown in the second line of Eq. (10), we end up with a redundant lower index which we can trace over, while at the left boundary we impose the condition that the two upper indices must be equal. The full influence functional can then be constructed by iteratively multiplying such matrix product operators. If we label the individual matrix product operators in the product by $G^{\alpha_i \dots \alpha_1}$, then we can express the iterative multiplication as

$$\mathcal{F}_{k:0}^{\alpha_k \dots \alpha_1} = \mathcal{G}_{\beta_{k-1} \dots \beta_1}^{\alpha_k \alpha_{k-1} \dots \alpha_1} \mathcal{F}_{k-1:0}^{\beta_{k-1} \dots \beta_1}, \quad (11)$$

with

$$\mathcal{G}_{\beta_{k-1} \dots \beta_1}^{\alpha_k \alpha_{k-1} \dots \alpha_1} := G^{\alpha_i \dots \alpha_1} \delta_{\beta_{k-1}}^{\alpha_{k-1}} \dots \delta_{\beta_1}^{\alpha_1}, \quad (12)$$

which is represented graphically by the two-dimensional ten-

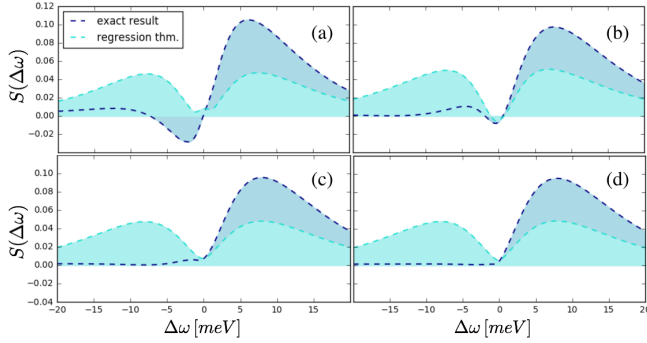


Figure 4. Phonon emission spectrum calculated using the local TEMPO algorithm as a function of SVD cutoff λ_c . We denote the local TEMPO calculated spectrum (with a certain fixed SVD cutoff) exact, and to gauge the importance of memory effects we compare this with a spectrum based on the quantum regression theorem which neglects correlations with the environment when computing intermediate dynamics. (a) $\lambda_c = 5 \times 10^{-4}$, (b) $\lambda_c = 5 \times 10^{-5}$, (c) $\lambda_c = 5 \times 10^{-6}$ and (d) $\lambda_c = 5 \times 10^{-7}$. The other simulation parameters are $\alpha = 1.3$, $\omega_c = 5\Omega$, $\nu = 1$, $\delta t = 0.05/\Omega$.

with dissipation strength α , cutoff frequency ω_c and Ohmicity ν , where for an Ohmic spectral density $\nu = 1$.

We quantify the computational complexity by the computation time required to contract a network of a certain size with a fixed singular value cutoff. This is dependent on the specific machine used, which we give details of in the Appendix. There, we also show that the time per iteration of the non-local TEMPO algorithm increases approximately linearly as the algorithm proceeds. In contrast, for a fixed network size and cutoff, the local TEMPO algorithm has a roughly constant time per iteration for most of the algorithm before slowly decreasing to zero. In Fig. 3, we plot the full computation time for the local and non-local representations as a function of dissipation strength. There, it can be seen that the local representation significantly outperforms the non-local one, and that the improvement increase with the couplings and as the singular value cutoff is decreased.

It should be recalled that the object we are computing is the full process tensor, which encodes all multi-time correlations, and from which a host of properties can be extracted. In particular, we can compute the steady state emission spectrum $S(\Delta\omega) = \text{Re} \left[\int_0^\infty d\tau (g^{(1)}(\tau) - g^{(1)}(\infty)) e^{-i\Delta\omega\tau} \right]$, defined in terms of the two-point correlation function $g^{(1)}(\tau) = \lim_{t \rightarrow \infty} \langle \sigma^\dagger(t + \tau) \sigma(\tau) \rangle$. The two-point correlation function is defined in terms of the raising and lowering operators on the spin system. We compute this function from the Choi state of the process tensor, constructed from the influence functional, using Eq. (3). To do so, we take all superoperators to be the identity superoperator \mathcal{I} (with action $\mathcal{I}[\rho] = \rho$) except for two, which append a raising or lowering operator respectively. In Fig. 4, we investigate the convergence of the local TEMPO algorithm with respect to the SVD cutoff value, by looking at the phonon emission spectrum. We compare this with correlation functions computed using the quantum regression theorem, which approximates intermedi-

ate dynamics with that from an initial product state and is valid in the weak-coupling limit [5]. The regression theorem correlations are obtained by breaking all correlations in the full process tensor Choi state across time steps at which the raising and lowering operators are evaluated.

We see that a high SVD cutoff predicts a negative part of the emission spectrum, which is unphysical. As the cutoff is increased the negative contribution vanishes, and the simulation appears well-converged for $\lambda_c = 5 \times 10^{-7}$. Additionally, we see that the converged exact spectrum predicts no emission at negative frequencies, this is in contrast to the regression theorem result which predicts a symmetric emission spectrum. This provides an illustration of the critical importance of accurately modelling memory effects.

Conclusion. – In this paper, we have established a direct connection between recent frameworks for characterizing general non-Markovian quantum processes and the path integral formulation of open dynamics. By relating the influence functional to a process tensor on an infinitesimal time grid, which has an explicit causal structure, we were able to build on recent progress in the classical simulation of Gaussian open quantum systems in terms of tensor networks. Specifically, we showed that the speed of the TEMPO algorithm, currently one of the leading numerically exact simulation methods, can be improved by several orders-of-magnitude, depending on the specific parameters, by shifting the boundary of the corresponding tensor network from a temporally non-local to a local one.

Expressing the influence functional as a component of the process tensor for a particular class of processes also highlights how it can be used to simulate experiments with interventions at multiple points in time. The ability to encode it as a quantum state, as in Eq. (8) makes the multi-time correlation functions it encodes, and their relation to approximations such as that made in the quantum regression theorem, more transparent. Moreover, putting discretized path integral techniques in a more general context indicates how they might be generalized to more complex system-environment interactions, or even beyond the Gaussian regime.

The power of the non-local TEMPO algorithm has been illustrated by computing the Ohmic localization transition, and the dynamics of complex problems with multiple separated timescales [31]. The improved method will be capable of exploring the same physics much more efficiently, and potentially explore problems outside the realm of the non-local formulation such as the sub-Ohmic localization transition. In addition, the freedom of boundary choice in Fig. 2, that we have identified here, could be further exploited in other contexts. While the local choice appears optimal here, it may be that for other, structured spectral densities, where there are recurrent correlations, other boundary choices could be more efficient. A point whose exploration we leave for future work.

In summary, our contribution is immediately applicable to the efficient simulation of realistic complex open systems, and in addition the reformulation illustrates the utility of thinking about a time-local propagation of a conditioned environment space, rather than a description resembling the

use of a non-local memory kernel. This conceptual point of view has proved fruitful here, and it is our hope that it might find broader use within open systems theory.

Acknowledgements. – FAP would like to thank A. Nazir, for asking one of the questions that motivated this work, and A. Strathearn, B. W. Lovett and P. Kirton for introducing and explaining the use of the TEMPO algorithm.

* matrj@fysik.dtu.dk

† felix.pollock@monash.edu

- [1] H. Breuer and F. Petruccione, *The Theory of Open Quantum Systems* (Oxford University Press, 2002).
- [2] U. Weiss, *Quantum Dissipative Systems* (World Scientific, 2012).
- [3] H. J. Carmichael, *Statistical Methods in Quantum Optics 1: Master Equations and Fokker-Planck Equations* (Springer, 2003).
- [4] C. A. Mujica-Martinez, P. Nalbach, and M. Thorwart, *Phys. Rev. E* **88**, 062719 (2013).
- [5] D. P. S. McCutcheon, *Phys. Rev. A* **93**, 022119 (2016).
- [6] D. Newman, F. Mintert, and A. Nazir, *Phys. Rev. E* **95**, 032139 (2017).
- [7] B. Vacchini and H.-P. Breuer, *Phys. Rev. A* **81**, 042103 (2010).
- [8] C. K. Lee, J. Moix, and J. Cao, *J. Chem. Phys.* **136**, 204120 (2012).
- [9] A. Fruchtmann, N. Lambert, and E. M. Gauger, *Sci. Rep.* **6**, 28204 (2016).
- [10] N. Makri and D. E. Makarov, *J. Chem. Phys.* **102**, 4600 (1995).
- [11] N. Makri and D. E. Makarov, *J. Chem. Phys.* **102**, 4611 (1995).
- [12] P. Nalbach, A. Ishizaki, G. R. Fleming, and M. Thorwart, *New J. Phys.* **13**, 063040 (2011).
- [13] N. S. Dattani, *AIP Adv.* **2**, 012121 (2012).
- [14] A. Strathearn, B. W. Lovett, and P. Kirton, *New J. Phys.* **19**, 093009 (2017).
- [15] Q. Shi and E. Geva, *J. Chem. Phys.* **119**, 12063 (2003).
- [16] G. Cohen and E. Rabani, *Phys. Rev. B* **84**, 075150 (2011).
- [17] J. Cerrillo and J. Cao, *Phys. Rev. Lett.* **112**, 110401 (2014).
- [18] F. A. Pollock and K. Modi, *Quantum* **2**, 76 (2018).
- [19] Y. Tanimura, *J. Phys. Soc. Jpn.* **75**, 082001 (2006).
- [20] J. Strümpfer and K. Schulten, *J. Chem. Theory Comput.* **8**, 2808 (2012).
- [21] R. Bulla, T. A. Costi, and T. Pruschke, *Rev. Mod. Phys.* **80**, 395 (2008).
- [22] A. W. Chin, Á. Rivas, S. F. Huelga, and M. B. Plenio, *J. Math. Phys.* **51**, 092109 (2010).
- [23] H.-T. Chen, G. Cohen, and D. R. Reichman, *J. Chem. Phys.* **146**, 054105 (2017).
- [24] H.-T. Chen, G. Cohen, and D. R. Reichman, *J. Chem. Phys.* **146**, 054106 (2017).
- [25] I. de Vega and D. Alonso, *Rev. Mod. Phys.* **89**, 015001 (2017).
- [26] R. Orús, *Ann. Phys.* **349**, 117 (2014).
- [27] F. A. Y. N. Schröder and A. W. Chin, *Phys. Rev. B* **93**, 075105 (2016).
- [28] M. L. Wall, A. Safavi-Naini, and A. M. Rey, *Phys. Rev. A* **94**, 053637 (2016).
- [29] F. A. Pollock, C. Rodríguez-Rosario, T. Frauenheim, M. Paterostro, and K. Modi, *Phys. Rev. A* **97**, 012127 (2018).
- [30] I. A. Luchnikov, S. V. Vintskevich, H. Ouerdane, and S. N. Filippov, [arXiv:1812.00043](https://arxiv.org/abs/1812.00043) (2018).
- [31] A. Strathearn, P. Kirton, D. Kilda, J. Keeling, and B. W. Lovett,

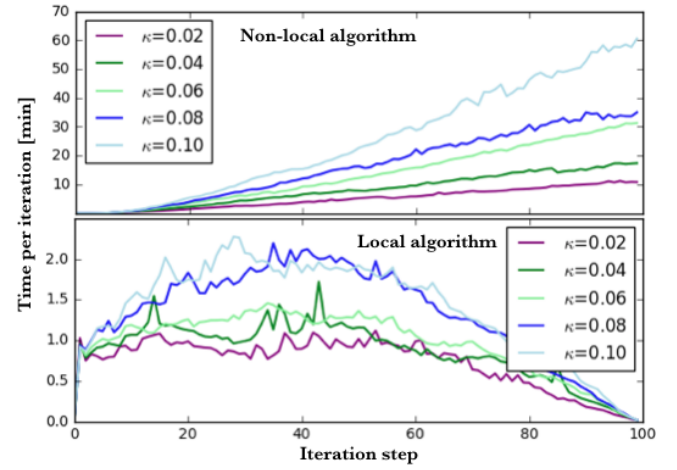


Figure 5. Comparison between scaling of the computation time per iteration for the local and non-local representations. The parameters used are $\alpha = \{0.02, 0.04, 0.06, 0.08, 0.10\}$, $\omega_c = 5\Omega$, $\nu = 1/2$, $\delta t = 0.05/\Omega$ and a singular value cutoff of $\lambda_c = 5 \times 10^{-7}$. Notice that two different axis scales are used and that, already at weak coupling, the local formulation outperforms the non-local one by a factor of up to 30.

Nat. Commun. **9**, 3322 (2018).

- [32] E. Sim and N. Makri, *Comput. Phys. Commun.* **99**, 335 (1997).
- [33] E. Sim, *J. Chem. Phys.* **115**, 4450 (2001).
- [34] N. S. Dattani, *Comput. Phys. Commun.* **184**, 2828 (2013).
- [35] L. Li, M. J. W. Hall, and H. M. Wiseman, *Phys. Rep.* **759**, 1 (2018), concepts of quantum non-Markovianity: A hierarchy.
- [36] S. Milz, F. Sakuldee, F. A. Pollock, and K. Modi, [arXiv:1712.02589](https://arxiv.org/abs/1712.02589) (2017).
- [37] F. A. Pollock, C. Rodríguez-Rosario, T. Frauenheim, M. Paterostro, and K. Modi, *Phys. Rev. Lett.* **120**, 040405 (2018).
- [38] L. Ballentine, *Quantum mechanics: a modern development* (World Scientific, 2014).
- [39] S. Milz, F. A. Pollock, and K. Modi, *Open Sys. Info. Dyn.* **1740016** (2017).
- [40] R. P. Feynman and F. L. Vernon, *Ann. Phys.* **24**, 118 (1963).
- [41] A. Atland and B. Simon, *Condensed matter field theory* (Cambridge University Press, 2010).
- [42] H. F. Trotter, *Proc. Amer. Math. Soc.* **10**, 545 (1959).
- [43] N. S. Dattani, F. A. Pollock, and D. M. Wilkins, *Quant. Phys. Lett.* **1**, 35 (2012).
- [44] U. Schollwöck, *Ann. Phys.* **326**, 96 (2011).
- [45] M. Buser, J. Cerrillo, G. Schaller, and J. Cao, *Phys. Rev. A* **96**, 062122 (2017).

APPENDIX

Generalized Choi-Jamiołkowski isomorphism. – The Choi state A of a superoperator \mathcal{A} is defined in terms of its action on one half of the maximally entangled state $\Psi = \sum_{jk} |jj\rangle\langle kk|/d$, where $\{|j\rangle\}$ forms an orthonormal basis for the d -dimensional system, as

$$A = \mathcal{A} \otimes \mathcal{I}[\Psi]. \quad (18)$$

In terms of this representation, the action on an initial state ρ can be written $\mathcal{A}[\rho] = \text{tr}_i[A \rho^T \otimes \mathbb{1}]$, where the trace is over

the first subsystem.

Similarly, the process tensor can be represented in terms of a many-body Choi state, defined on the space of the original system and $2k$ ancillas [39]; it encodes all uncontrolled features of the process, and is given by

$$\Upsilon_{k:0} = \text{tr}_E (\mathcal{U}_{\delta t} \dots \mathcal{U}_{\delta t} [\Psi^{\otimes k} \otimes \chi_0]) , \quad (19)$$

where now the k 'th unitary acts on the environment space and one part of the k 'th maximally entangled ancilla state. Action on a sequence of superoperators involves contraction with the tensor product of the transposes of their Choi states, as in the main text.

The generalized Choi state can be physically realized by choosing each superoperator intervention as a SWAP operation between the system and one part of a bipartite maximally entangled ancilla. The resulting state encodes all temporal correlations of the process as spatial correlations in the ancillary space.

Explicit form of influence tensors. – Recall that the influence tensors connect the dynamics around time step i with that around step j . For linearly coupled models, the individual tensors $[b_i]$ depend only on the temporal separation $l\delta t$. The influence tensors are given by [14, 31]

$$[b_{(i-j)}]^{\alpha_i \alpha_j} = e^{-(s_i - r_i)(\eta_{i-j} s_j - \eta_{i-j}^* r_j)} , \quad (20)$$

expressed in terms of the memory kernel elements

$$\eta_{i-j} = \begin{cases} \int_{t_{i-1}}^{t_i} \int_{t_{j-1}}^{t_j} dt' dt'' C(t' - t'') , & i \neq j \\ \int_{t_{i-1}}^{t_i} \int_{t_{i-1}}^{t_i} dt' dt'' C(t' - t'') , & i = j \end{cases} , \quad (21)$$

which are themselves defined in terms of the bath auto-

correlation function

$$C(t) = \int_0^\infty d\omega J(\omega) \left[\coth\left(\frac{\beta\omega}{2}\right) \cos(\omega t) - i \sin(\omega t) \right] . \quad (22)$$

The bath auto-correlation function is given in terms of the environment spectral density $J(\omega)$ introduced in the main text.

Scaling comparison. – In Fig. 5, we compare the computation time per iteration of the non-local and the local network representations, for a fixed network size and SVD cut-off. We see that the time per iteration of the non-local tempo algorithm increases approximately linearly. For a finite network, the local tempo algorithm has a time per iteration which rapidly goes to a non-increasing value. The growth of complexity in the non-local case is mainly due to the build up of irrelevant information, rather than a genuine build-up of temporal correlations. The observed decrease in the computation time per iteration for the local case, is a consequence of working with a finite network. In the original TEMPO proposal [31], it was argued that one could implement a truncation of the number of tensors in the propagators and obtain a constant scaling at long times. The same method could be applied with the local tempo algorithm, only with a significantly reduced time per iteration. More rigorously, we could combine the tools developed here with the transfer tensor approach [17, 18, 45], which infers long-time correlations from a short-time simulation. The problem would then become efficiently contracting the full network up to a sufficiently long-time.

Specific machine and implementation. – All the simulations presented in this work were carried out on a 2011 MacBook Pro with a 2.4 GHz Intel Core i5 processor and a 4GB 1333 MHz DDR3 memory. The algorithm has been implemented using the programming language Python, no specialized packages, beyond NumPy, were used. There is extensive scope for optimization, and utilizing packages for tensor network manipulations could conceivably make the implementation easier.